ACS NANO

www.acsnano.org

ARTICLE

Correlated Lattice Fluctuations in $CsPbBr_3$ Quantum Dots Give Rise to Long-Lived Electronic Coherence

Arnab Ghosh, Albert Liu,* Simon C. Boehme, Patrick Brosseau, Dmitry N. Dirin, Maksym V. Kovalenko, and Patanjali Kambhampati*

Cite This: *ACS Nano* 2025, 19, 19927−19937

Read Online

ACCESS | Metrics & More | Article Recommendations | Supporting Information

ABSTRACT: **Electronic coherence is central to numerous areas of science, from quantum biology to quantum materials. In quantum materials, lead-halide perovskite (LHP) quantum dots (QDs) have been shown to support electronic coherence through observation of coherent single-photon emission and superfluorescence arising from spatial coherence at low temperatures. In contrast, direct measurement of temporal coherence between exciton states has been lacking. Here, we employ coherent multi-dimensional spectroscopy to observe an electronic coherence between exciton states in $CsPbBr_3$ QDs that is long-lived at room temperature, surviving nearly three times longer than the electronic dephasing time. This observation of a long-lived electronic coherence at room temperature points to nearly perfectly correlated lattice fluctuations for each excitonic state in the superposition. These experiments reveal that the properties of LHP QDs extend to lattice dynamics that give rise to correlated fluctuations in the basis exciton states, a process that may next be optimized by design.**

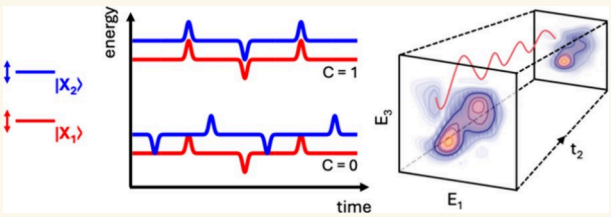

KEYWORDS: *lead-halide perovskite, quantum dot, nanocrystal, coherent multidimensional spectroscopy, two-dimensional electronic spectroscopy, electronic coherence*

INTRODUCTION

Coherence between quantum states is general feature of quantum materials and their deployment in quantum enabled technologies.[1,2] The coherences observed historically are low energy (millielectron-volts), arising from phonons,[3−5] spins,[6,7] or exciton fine structure[8] as the basis states. For wide deployment of quantum technologies, however, quantum coherence that extends to higher energies and that operates at room temperature are urgently needed. The former requirement has been met in various quantum systems, but implementing quantum technologies under ambient conditions is typically prohibited by the fragility of quantum states and the ubiquitous sources of decoherence that are most severe at room temperatures.

A system that has attracted tremendous attention for their quantum optoelectronic properties is the lead-halide perovskite (LHP) quantum dots (QD).[9,10] For example, demonstrations of single-photon emission, superfluorescence, and coherent spin manipulation all point to LHP QDs as a promising material platform for a wide variety of quantum applications. These LHP QDs further offer facile chemical synthesis, offering both scalability and straightforward integration into various quantum technologies. Yet most of their quantum emitter phenomena are, as is common in quantum materials more generally, observable only at cryogenic temperatures since strong coupling between charge carriers and the underlying perovskite lattice is both responsible for many of their unique characteristics, and conversely the very source of quantum decoherence at elevated temperatures.[2,5,7,11−13]

Here, we report on the first observation of long-lived electronic coherence in $CsPbBr_3$ LHP QDs. We employ broadband Coherent Multi-Dimensional Spectroscopy (CMDS) to measure coherent oscillations at the frequency of an excitonic splitting, not overlapping with any phonon coherences. Two-dimensional amplitude and phase correlation maps unambiguously reveal the observed coherence to be electronic. The electronic coherence is shown to be long-lived even at room temperature, with a dephasing time of 119 fs that is nearly three times longer than the pure electronic dephasing

Received: February 19, 2025
Revised: May 9, 2025
Accepted: May 12, 2025
Published: May 19, 2025

https://doi.org/10.1021/acsnano.5c03051
ACS Nano 2025, 19, 19927−19937

time of the basis excitonic states. This long-lived electronic coherence survives due to correlated fluctuations in the LHP lattice that persist despite the system being warm and wet.

RESULTS AND DISCUSSION

The system we study is $CsPbBr_3$ QDs,[14,15] which exhibits an orthorhombic crystal structure at room temperature as shown in Figure 1a. All figures and discussion are for QDs with edge

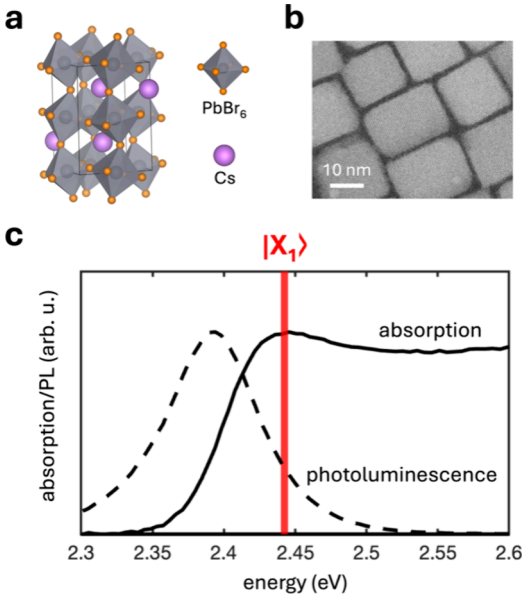

Figure 1. Linear optical properties of $CsPbBr_3$ quantum dots. (a) Crystal structure of $CsPbBr_3$ in an orthorhombic crystal phase at room temperature. (b) Transmission electron micrograph of $CsPbBr_3$ QDs, informing an average side length of 18 nm. (c) Absorption and photoluminescence spectra of the 18 nm $CsPbBr_3$ QDs, exhibiting a single absorption peak by the band-edge exciton state $|X_1\rangle$ and a single Stokes-shifted emission peak from the same transition.

lengths of 18.4 nm (informed by the transmission electron micrographs shown in Figure 1**b**), though we repeated our experiments and analysis for smaller QD with 4.9 and 9.4 nm edge lengths and observed the same quantum coherence at room temperature (see Supporting Information Table S1).

The linear optical properties of our system are shown in Figure 1c, which exhibit an absorption peak at 2.43 eV and Stokes-shifted photoluminescence at 2.39 eV consistent with previous studies of comparable samples.[15−23] These one-dimensional spectra resolve only one single low-energy excitonic state, denoted here as $|X_1\rangle$. Higher-energy excitonic states remain unresolved in the absorption spectrum due to the combination of (i) small energetic separations between subsequent transitions in such large and weakly confined QDs, and (ii) significant peak broadening, arising from both the pronounced exciton−phonon coupling in $CsPbBr_3$ QDs at room temperature and an inhomogeneous peak broadening contribution from a finite QD size and shape distribution of the probed QD ensemble.[15] Higher-energy excitonic states are also not observed in the photoluminescence spectrum due to exciton relaxation to $|X_1\rangle$ proceeding orders of magnitude faster than radiative decay,[24] typically occurring on a subpicosecond (see SI) and nanosecond time scale in $CsPbBr_3$ QDs at room temperature, respectively. Consequently, any potentially present interexcitonic coherence between excited states at room temperature remain concealed in ensemble measurements usings such one-dimensional absorption and photoluminescence spectroscopy.

Here, we leverage the unique capabilities of CMDS toward circumventing the above limitations of linear and one-dimensional techniques. CMDS has proven powerful in disentangling complex dynamics in varied condensed, chemical, and biological systems,[25,26] and has also been applied to LHP QDs more recently.[27,28] However, previous applications of CMDS to LHP QDs have largely applied limited excitation spectral bandwidth,[28] sufficient only to study the band-edge exciton dynamics. Here, we implement broadband CMDS with excitation pulses generated from a hollow-core fiber (as previously described). As the resulting excitation bandwidths of 300 meV exceeds intraband level spacings in CsPbBr3 QDs, we can capture both the band-edge exciton and higher-lying excitons simultaneously.

A schematic of our CMDS experiment is shown in Figure 2**a**, in which three excitation pulses with variable interpulse

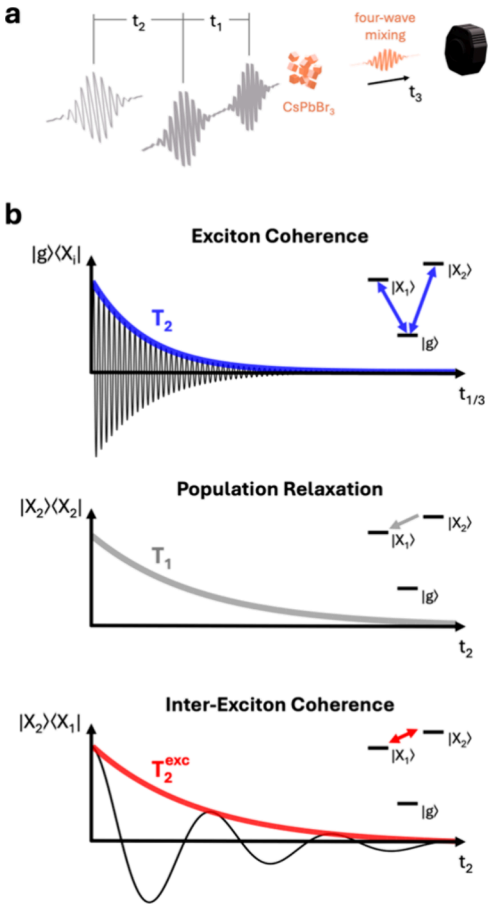

Figure 2. Nonlinear four-wave mixing spectroscopy reveals dephasing and relaxation times. (a) Experimental schematic of coherent multidimensional spectroscopy, involving initial excitation of the $CsPbBr_3$ QD ensemble by two collinear pulses separated by a time delay t_1, followed by a third pulse after an intermediate time delay t_2. The three excitation pulses generate a four-wave mixing signal that emits along the real laboratory time t_3. (b) Optical exciton coherence evolves along the time delays t_1 and t_3, while population relaxation and interexciton coherence between two excited states evolve along the intermediate time delay t_2.

https://doi.org/10.1021/acsnano.5c03051
ACS Nano 2025, 19, 19927−19937

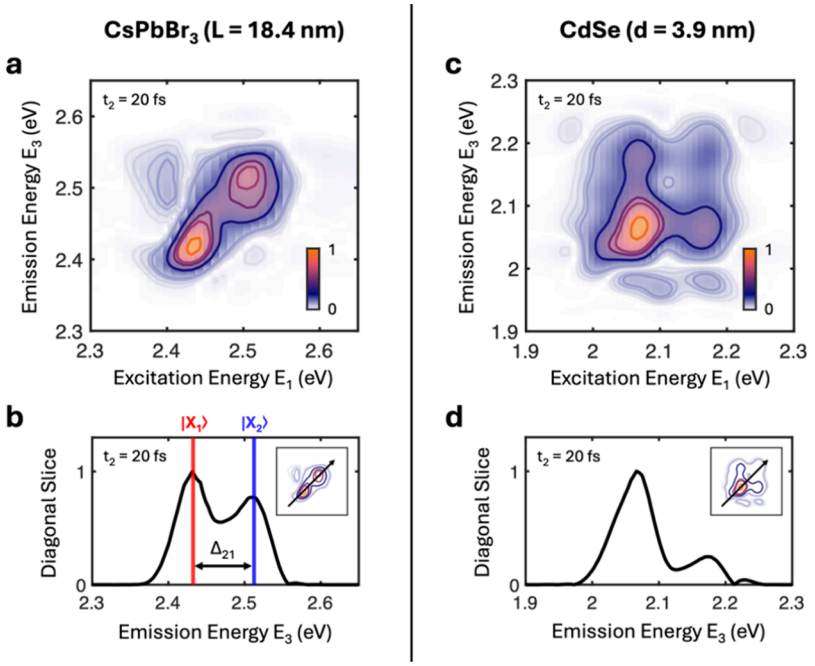

Figure 3. Nonlinear multidimensional spectroscopy reveals two excitonic states to form a basis for electronic coherences. (a). Absorptive CMDS spectrum acquired at a time-delay t_2 = 20 fs exhibits a complex structure absent in one-dimensional spectra for 19 nm $CsPbBr_3$ QD. (b) Lineshape along the energy "diagonal" direction ($E_1 = E_3$) as indicated inset, which reveals two peaks corresponding to two states $|X_1\rangle$ and $|X_2\rangle$ separated by an energy splitting Δ_{21} = 80 meV. $|X_1\rangle$ is the familiar band-edge exciton manifold while $|X_2\rangle$ is a new excitonic state revealed by CMDS. (c) CMDS spectrum of 3.9 nm diameter CdSe QD. (d) Diagonal projection of the CdSe spectrum.

time delays t_1 and t_2 generate a nonlinear four-wave mixing (FWM) signal that emits along the real laboratory time t_3. The evolution of the FWM signal as a function of each time delay then provides unique information concerning the dynamics of the system density matrix as shown in Figure 2b. In the top panel, dynamics of interband coherences between the electronic ground state $|g\rangle$ and an exciton state $|X_i\rangle$ evolve across the time delays t_1 and t_3, which decay with a dephasing time $T_2^{X_i}$. Across the remaining intermediate time delay t_2, two distinct processes contribute. In the middle panel, decay of excited-state populations occurs with a relaxation time $T_1^{X_i}$, which can occur due to radiative relaxation into the ground state (which we neglect here due to the nanosecond time scale) and also between exciton states (femto- to picosecond time scale). In the bottom panel, interexcitonic quantum coherences between distinct exciton states $|X_i\rangle$ and $|X_j\rangle$ (with an energy separation within the excitation bandwidth) decay with a dephasing time T_2^{exc}.

Guided by the correspondence between each time delay and the dynamics of quantum coherences and populations, we are now in a position to design a CMDS experiment to completely characterize the quantum dynamics of our $CsPbBr_3$ QDs. To perform CMDS, we measure the FWM signal along the time delays $\{t_1,t_3\}$S and Fourier transform along both time axes to correlate their corresponding excitation and emission dynamics. A resultant absorptive two-dimensional spectrum is shown in Figure 3a for an intermediate time delay t_2 = 20 fs, which exhibits a rich structure absent in one-dimensional absorption and photoluminescence spectra. We may immediately examine its line shape along the 'diagonal' ($E_1 = E_3$) line, which is plotted in Figure 3b and exhibits two distinct peaks. Given that this line shape reflects optical excitation and stimulated emission at identical photon energy $E_1 = E_3$, we may loosely interpret the spectrum in Figure 3b as a 'nonlinear' electronic density of states and identify the lower-energy peak as the familiar band-edge exciton $|X_1\rangle$ (at an energy E_{X1} = 2.43 eV) and the higher energy peak as a new exciton state $|X_2\rangle$ (at an energy E_{X2} = 2.51) hidden in both the linear optical spectra shown in Figure 1c and previous transient absorption spectra. This is the diagonal (D) spectrum of a CMDS data set.

Shown in Figure 3**c-d** are the spectra for 3.9 nm diameter CdSe QD as a reference for QD with a spectrum of excitons that may support electronic coherence, moreover one that is long-lived. The CMDS data in Figure 3c shows that there are also two exciton states that lie within the pump bandwidth. These two states are the well-known 1S and 2S exciton states in the multiband effective mass approximation.[29,30] Although recent empirical pseudopotential calculations reveal more states present with slight differences in their excitonic nature.[31,32] Figure 3d shows the D spectra illustrating two well-resolved excitonic states for which a coherence may be formed.

The two-dimensional lineshapes of each peak then allow us to characterize the intrinsic dephasing times of each exciton transition. It is these phase and population relaxation times that set the speed limits on electronic coherence and that it is long-lived relative to some speed limit. Specifically, Figure 4a displays the 'antidiagonal' (AD) lineshapes of the $|X_1\rangle$ and $|X_2\rangle$ transitions, whose cross-diagonal line widths return dephasing times of T_2 = 55 fs and T_2 = 34 fs for the $|X_1\rangle$ and $|X_2\rangle$ transitions, respectively. We note that dephasing times were extracted from spectra at short intermediate time delay t_2 = 20 fs to avoid broadening effects due to spectral diffusion and/or polaron formation.[27,33]

With knowledge of the two exciton transitions and their intrinsic dynamics in hand, we can leverage the additional t_2 degree of freedom to probe system dynamics ranging from zero frequency (population relaxation) up to frequencies

https://doi.org/10.1021/acsnano.5c03051
ACS Nano 2025, 19, 19927−19937

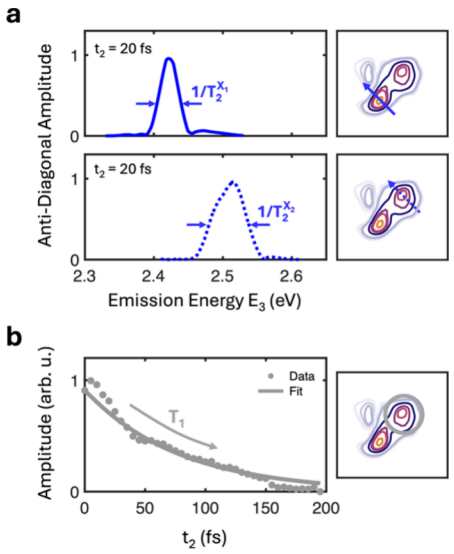

Figure 4. Measuring phase and population relaxation to identify speed limits for possible electronic coherence. (a) Antidiagonal (AD) spectrum for the $|X_1\rangle$ state, which only has phase relaxation. Antidiagonal (AD) spectrum for the $|X_2\rangle$ state, which includes population relaxation. (b) Measurement of population relaxation from $|X_2\rangle$ to $|X_1\rangle$.

within the excitation bandwidth (interexciton coherence), as shown in Figure 4b. To measure population relaxation, decay of the 2-D spectrum amplitude at a coordinate $(E_1,E_3) = (E_{X2},E_{X1})$, corresponding to excitation at the higher-lying exciton $|X_2\rangle$ and emission at the lower-lying exciton $|X_1\rangle$, returns an $|X_2\rangle$ population relaxation time of T_1 = 78 fs (SI). Radiative relaxation of each exciton to the electronic ground state $|g\rangle$ occurs on far longer (nanosecond) time scales and is thus neglected in the remaining analysis. We have recently performed detailed energy resolved CMDS analysis of hot exciton cooling dynamics,[16] consistent with this measurement.

To measure coherence from a superposition of exciton states, we consider positions in the CMD spectra corresponding to excitation and emission involving different exciton transitions. While this includes the same spectral coordinate $(E_1,E_3) = (E_{X2},E_{X1})$ from above, the simultaneous presence of population relaxation complicates analysis of any underlying coherent dynamics. We therefore consider the inverse position $(E_1,E_3) = (E_{X1},E_{X2})$, corresponding to excitation at the lower-lying exciton $|X_1\rangle$ and emission at the higher-lying exciton $|X_2\rangle$, which isolates possible signatures of interexcitonic coherence along the time delay t_2 as shown schematically in Figure 5**a.**

Whereas there have been searches for electronic coherence in quantum materials and QD, these are low energy, requiring cryogenic temperatures; there have been no observations of electronic coherence from a basis of exciton states. In contrast, in biophysical systems like photosynthetic light harvesting complexes and their analogs, there has been a long search for electronic coherences arising from exciton states via CMDS. This search for electronic coherence focused on the idea of long-lived coherences arising from correlated motions among excitons.[34−38] Following the initial reports to the positive,[39−44] there have been other reports to the negative.[37,45,46,38] The search for electronic coherence in these systems was initially reported in several examples, but these examples are suggested to arise from other effects such as vibronic coherence. For an inorganic system with perfect order, nanoplatelets have shown excitonic electronic coherence.[47] As we discuss further below in comparing $CsPbBr_3$ to CdSe QD, the presence of excitonic peaks does not guarantee the observation of electronic coherence let alone that it is long-lived. There are key issues of disorder that must be addressed.

We now arrive at the primary result of this work, namely the electronic coherence in a warm and wet (more precisely a

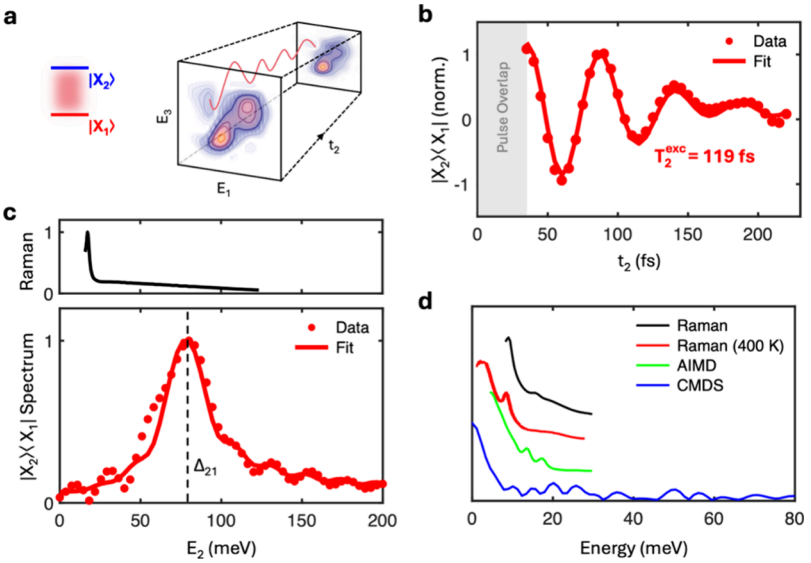

Figure 5. Correlated fluctuations preserve interexcitonic coherence at 300 K. (a) A coherent superposition of the two exciton states $|X_2\rangle\langle X_1|$ evolves along t_2 at the coordinate $(E_1,E_3) = (E_{X1},E_{X2})$. (b) Experimental measurement of the interexciton coherence at room temperature in 18 nm $CsPbBr_3$ QD from which a coherence time of T_2^{exc} = 119 fs is fitted. (c) Its Fourier transform returns an oscillation frequency of 80 meV, matching the exciton energy splitting. Shown also is a Raman spectrum adapted from,[56] which demonstrate that the electronic coherence exists at an energy splitting for which there are no vibronic/phonon coherences. (d) Low frequency Raman spectra showing the spectral density of the lattice bath. The Raman spectra are adapted with permission from ref 55. Copyright 2017 American Physical Society. The AIMD spectra are adapted with permission from ref 57. Copyright 2024 arXiv.

https://doi.org/10.1021/acsnano.5c03051
ACS Nano 2025, 19, 19927−19937

lattice with liquid-like structural dynamics[27,33,48−55]) material is long-lived relative to the intrinsic time scale limited by pure electronic dephasing. The experimental t_2 dependence of the CMD spectrum at $(E_1,E_3) = (E_{X1},E_{X2})$ (following a Fourier filtering procedure to remove a slowly varying background (as detailed in the SI) is shown in Figure 5b, which exhibits clear coherent oscillations indicative of quantum coherence. A fit of the oscillation in the time-domain then returns a coherence time of T_2^{exc} = 119 fs. Its Fourier spectrum then reveals an oscillation frequency matching the energy splitting Δ_{21} = 80 meV between $|X_1\rangle$ and $|X_2\rangle$, as expected from a superposition between the two basis exciton states, Figure 5c. Also shown in Figure 5**c** is a Raman spectrum adapted from[56] which demonstrates that the electronic coherence exists at an energy splitting for which there are no vibronic/phonon coherences. In the early examples of interexcitonic electronic coherence, the coherence was later shown to be of vibronic origin. With these data, we can clearly show that the putative electronic coherence has no Raman vibronic coherences at the same energies.

Figure 5**d.** shows the low frequency Raman spectra to show the spectral density of the lattice bath. The Raman and AIMD spectra are adapted from.[55,57] The main idea from these Raman spectra is that the response is a spectral density at 300 K, characteristic of overdamped phonon modes undergoing anharmonic mixing to produce a lattice response that is similar to a liquid or glass, unlike CdSe QD or other covalent semiconductors. This phonon spectral density represents the lattice motions to which the excitons couple. Rather than undergoing periodic modulation, the excitons undergo fluctuations by coupling to the fluctuating lattice bath.[13,15,27,33,49,54,55,58,59]

While it may not seem surprising that a basis of exciton states supports electronic coherence, closer scrutiny reveals divergence from this simple view. The behavior of the $CsPbBr_3$ QD here is compared to the same search for coherences in CdSe QD.[60] CdSe QD are actually a more ideal system for supporting electronic coherence, upon initial inspection. CdSe QD have well-resolved excitonic states easily spanned in CMDS experiments.[31,32,61−65] Yet an electronic coherence was not observed, while a vibronic coherence was observed.[60] This situation of observing one coherence but not the other, is precisely inverted from the behavior of the LHP QD.

Figure 6 illustrates the CdSe response in which there are vibronic coherences but not interexcitonic electronic coherences. The data is adapted from.[60] Figure 6a shows the idea of observing interexcitonic coherences in CdSe QD. Unlike CsPbBr3 QD, these conventional CdSe QD show two peaks within the light source spectrum. These peaks arise from well understood excitonic states that are nominally described via multiband effective mass theories,[66,67] but are better described using atomistic theories.[31,32,60,68−74] Here, the simple level diagram in Figure 2 is extended to include coupling to phonons since they are easily seen in experiment.[75,76]

Figure 6b shows the residual oscillations from the CMDS data, with spectral selection of E_1 to be resonant with the X1 state. There are clear oscillations in the data. Figure 6c shows the Fourier transform of the residual oscillations to compare to Raman and electronic spectra. These CMDS experiments reveal a clear vibronic coherence, matching with the energies of the optical and acoustic phonons in CdSe QD. The lines are broader than obtained with transient absorption spectroscopy only due to those experiments sampling the coherence for 10 ps, with a 5 ps decay time, whereas these CMDS experiments only extend to 500 fs so cannot as well resolve the phonon modes. The energy of a putative interexcitonic electronic coherence is shown, but it does not appear in the experimental data. Hence a QD system that initially appears better suited to observing electronic coherence is actually far worse at supporting this form of coherence. Clearly there is something unique about the excitonic structure of these basis states in LHP QD, and there is also unique character to their dynamically disordered lattice which better protects the electronic coherence from dephasing than the ordered covalent lattice of CdSe QD.

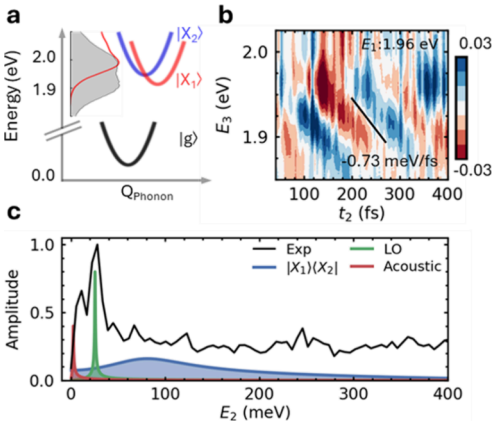

Figure 6. CdSe QD show vibronic coherence but no interexcitonic electronic coherence. (a) Low-energy linear absorption of 3.9 nm diameter CdSe QD revealing two excitonic states. (b) Residual oscillations from CMDS data. (c) Fourier transform of the residual oscillations. The AIMD spectra are adapted with permission from ref 60. Copyright 2021 National Academy of Sciences.

The rationalization for this absence of electronic coherence in CdSe QD emerged from *ab initio* molecular dynamics simulations.[60] The main idea is that the spectroscopic observation of two resolved peaks does not guarantee the basis states supporting a coherence. The reason is that there are in reality many more basis states[31,32,77,78] than implied by the presence of two peaks. Moreover these basis states undergo fluctuations which may induce dephasing as for CdSe QD or may protect from dephasing to support coherences. Finally such a coherence protection mechanism may enable an electronic coherence to be long-lived relative to the internal speed limits of phase and population relaxation times of the basis exciton states.

In the search for electronic coherences in condensed phase systems, especially in biological systems, a key issue is to ensure that the putative electronic coherence does not overlap with a Raman spectrum of the coupled vibrational modes. The oscillations in the CMDS data reveal a coherence that is likely to be interexcitonic in origin by virtue of the oscillation frequency matching the peak splitting for the two excitons in the basis. The lack of overlap between the putative interexcitonic electronic coherence and the vibronic coherences further support this assignment. The most detailed characterization to distinguish electronic from vibronic coherences 2D correlation maps of phase and amplitude.[60,79−82]

These correlation maps are shown in Figure 7 the putative electronic coherence in these perovskite QD and for a phonon coherence in CdSe QD. The details of the modeling can be

https://doi.org/10.1021/acsnano.5c03051
ACS Nano 2025, 19, 19927−19937

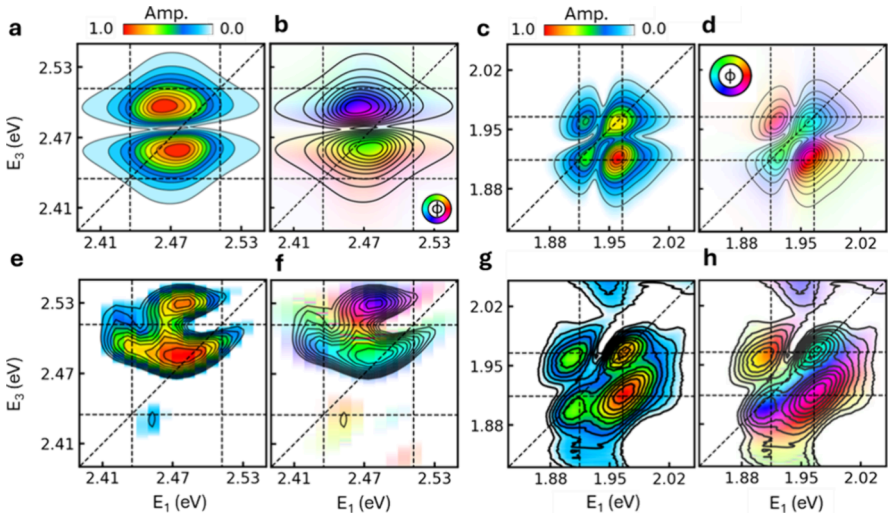

Figure 7. Two-dimensional amplitude and phase correlation maps unambiguously assigns the nature of coherences as electronic or vibronic. The simulated coherence maps are shown in the top row, (a−d) The experimental coherence maps are shown in the bottom row. (e−h) Across each row are the simulated and experimental coherence maps for electronic coherence (amplitude), electronic coherence (phase), vibronic coherence (amplitude), and vibronic coherence (phase). CdSe data adapted with permission from ref 60. Copyright 2021 National Academy of Sciences.

found in our previous work on the search for electronic coherence in QD.[60] Briefly, we used multimode Brownian oscillator model which assumes the line shape functions can be decomposed in a sum of contributions from multiple uncorrelated bath modes.[83] The model coherence map for electronic coherence is obtained by considering a four-level system consisting of a ground state |G>, two excitons states |X_1>, |X_2> and a biexciton state, |XX>. The difference in energy between these two exciton states sets the frequency of the oscillation along e_2.The model coherence map for vibrational coupling is obtained by considering a three-level system consisting of a ground state |G>, a single exciton state |X_1>, and a biexciton state |XX>. Coupling to vibrations is modeled as an undamped classical vibrational bath mode (e_{vib} = 25.5 meV) using the Huang−Rhys line shape function with S = 0.2 at 300 K.

As discussed in our original work using these coherence maps,[60] a minimal spectroscopic model of QD requires inclusion of excited state absorption from excitons to biexcitons. Fortunately there is a basis of understanding the spectroscopy of biexcitons in QD based upon time-resolved photoluminescence spectroscopy,[17,19,20,23,62,84] transient absorption spectroscopy,[30,62,77,85−90] and coherent multidimensional spectroscopy.[62,64] While there is electronic structure to biexcitons as there is to the basis excitons, for these bandwidths and temperatures one only needs to consider one absorbing biexciton state. Based upon this modeling, there is excellent consistency between the experiment and simulation. These results demonstrate that electronic and vibronic coherences can be qualitatively distinguished based upon two-dimensional coherence maps.

The size dependence of the coherence further supports its origin as due to correlated excitons coupled to the lattice bath. All QD show spectra of confined excitons.[30,66,78] LHP QD are no different, with a band edge exciton energy and an S−P energy gap that follows an inverse power law functional form.[12,15] This |X_2> state observed here, contributing to the |X_2>< X_1|coherence, has not been observed in linear absorption or transient absorption. CMDS has revealed this higher lying state,[16,33] with preliminary experiments revealing an anomalous size dependence in the opposite direction of standard quantum size effects.

Assuming this higher-lying exciton is an excitation-induced state, it would not appear in the linear absorption spectrum. Moreover this state may not be visible in transient absorption spectroscopy due to it being a one-dimensional spectroscopy that suffers from spectral congestion as discussed in the CMDS literature.[25,26,35,91−93] We have recent reports in which CMDS revealed these two peaks in LHP QD and enabled characterization of their relaxation dynamics[16,33] and nonlinear optical signals,[61] but they do not explain the physical origin. The physical origin of this higher-lying state is currently being investigated. For the present purposes, we can say that there are two observed peaks in the frequency domain and one coherence period in the time domain representation.

The size dependence is shown in Figure 7a. The peak splitting in the frequency domain as well as the oscillation frequency in the time domain have a clear linear relationship to the QD edge length. This linear relationship is not just quantitatively different than standard QD response, but is qualitatively different; it is in the opposite direction. Nonetheless, there is observation of electronic coherence in three different lengths of $CsPbBr_3$ QD, with a strong size dependence (Figure 8). The oscillation amplitude also maintains this strong, linear edge length dependence, Figure 7b.

This inverse size dependence to the splittings and coherence amplitude suggests that these effects are not standard QD size effects. Instead, these effects may arise from an excitation induced process. One example of such a process arises from exciton-polaron coupling. In lieu of exciton−phonon coupling for CdSe QD, LHP QD have exciton-polaron coupling as the appropriate electron−lattice interaction picture. We have suggested via simpler time-resolved photoluminescence[17,20] and transient absorption spectroscopy[48] that strong exciton-polaron coupling should give rise to polaron induced localization of the exciton. Recent work by linear spectroscopy and *ab initio* molecular dynamics simulations further

https://doi.org/10.1021/acsnano.5c03051
ACS Nano 2025, 19, 19927−19937

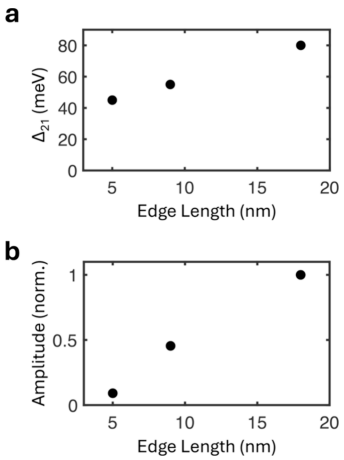

Figure 8. Generalizing the electronic coherence to other QD side lengths. (a) Interexcitonic energy splitting vs side length. (b) Interexcitonic oscillation amplitude relative to the baseline signal vs edge length.

corroborates this picture.[57] Very strong exciton-polaron coupling may then give rise to an excitation induced spectrum of states.

The simplest inspection of a quantum system suggests that a coherent superposition of basis states will produce a coherence. Coherences have been seen in many degrees of freedom. But as we showed in comparing LHP QD to II−VI QD, the presence of peaks in a linear absorption spectrum is not a guarantee that an electronic coherence will exist. Moreover, if an electronic coherence exists, it will diphase. But will this dephasing time scale be long relative to the internal speed limits set by T_2 of each state? Figure 9 addresses this final question of why this interexcitonic electronic coherence is long-lived.

Assuming two exciton transitions that experience uncorrelated energetic fluctuations that induce dephasing, the interexciton coherence time T_2^{exc} is shorter than those of the individual exciton transitions, related by $T_2^{exc} = \left[\frac{1}{T_2^{X_1}} + \frac{1}{T_2^{X_1}}\right]^{-1}$. The drastic difference between the long interexciton coherence time observed in our experiments and the far shorter interexciton coherence time naively expected from uncorrelated transitions (21 fs with the exciton dephasing times given above) may be reconciled, however, if their underlying fluctuations are correlated. The above relation between the interexciton coherence time and the intrinsic exciton coherence times are now generalized in the following relation (see[47] for details and derivation):

The above relation between the interexciton coherence time and the intrinsic exciton coherence times are now generalized in the following relation:

$$T_2^{exc} = \left[\frac{1}{T_2^{X_1}} + \frac{1}{T_2^{X_1}} - \frac{2C}{\sqrt{T_2^{X_1}T_2^{X_2}}}\right]^{-1} \quad (1)$$

where C is a coefficient that reflects the degree of correlation between the fluctuations of $|X_1\rangle$ and $|X_2\rangle$, ranging from −1 (perfectly anticorrelated) to 1 (perfectly correlated) and becoming zero for uncorrelated fluctuations as illustrated in Figure 9a.

To confirm that synchronized fluctuations are responsible for the remarkably long-lived quantum coherence we observe at room temperature, we perform a classical simulation of the interexciton coherence dephasing (valid at the high temperature considered here) by generating 10000 trajectories of each exciton energy $E_{X1}(t)$ and $E_{X2}(t)$ in time for a given degree of correlation to perform a subsequent ensemble average. The results of these simulations are shown in Figure 9b which indicate that for uncorrelated fluctuations (C = 0) the interexciton coherence dephases immediately as expected from the prior discussion while for the near-perfectly correlated fluctuations inferred from our experimental measurements (C = 0.96) the interexciton coherence persists on a time scale compatible with the experimental measurements. The Fourier spectrum shown in Figure 9c. These simulations well reproduce the experiments by invoking near perfect correlation between the fluctuations each state experiences by coupling to the lattice bath.

CONCLUSIONS

To conclude, these CMDS measurements reveal that electronic quantum coherence between exciton states in LHP QDs can persist at room temperature, for time scales far exceeding optical coherence times. This quantum coherence involves two excitonic states revealed by coherent multidimen-

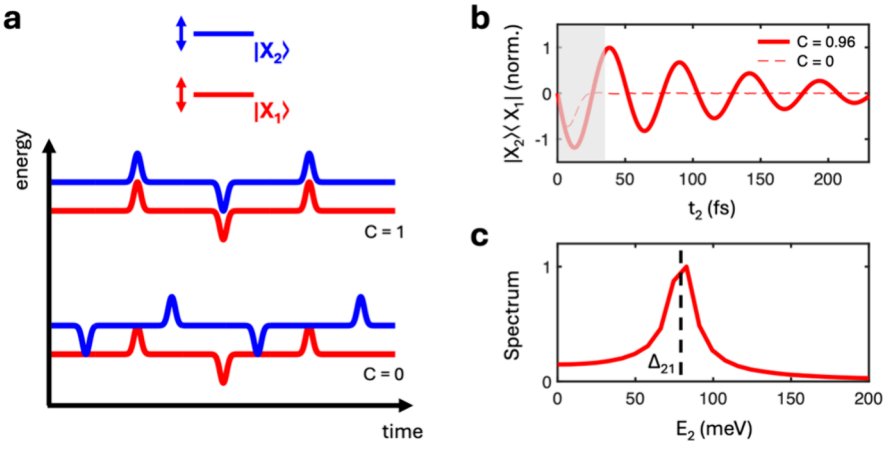

Figure 9. Correlated fluctuations give rise to long-lived electronic coherence. (a) Illustration of a two-state system undergoing fluctuations with and without correlations. (b) Simulated electronic coherence. (c) Lineshape of the simulated electronic coherence.

https://doi.org/10.1021/acsnano.5c03051
ACS Nano 2025, 19, 19927−19937

sional spectroscopy, whose energetic fluctuations are remarkably synchronized even at warm and wet conditions of an anharmonic lattice at room temperature. These findings pave the way to leverage this room temperature quantum coherence toward extending the transformative quantum applications of LHP QDs to higher temperatures enabled by higher energy coherences.

METHODS

The methods, materials, and simulations are detailed in the SI. Briefly, the CMDS experiments were performed in the pump/probe geometry. The light source was an Ar filled hollow core fiber pumped with an optical parametric amplifier. The coherent pulse trains were generated by acousto-optic modulators. The CMDS experiment has been detailed in our prior works on method development[61,94−98] and application of CMDS to QD.[16,27,31−33,60,64,65] The LHP QD were synthesized as described previously.[15]

ASSOCIATED CONTENT

Supporting Information

The Supporting Information is available free of charge at https://pubs.acs.org/doi/10.1021/acsnano.5c03051.

Synthesis and characterization of LHP QD, CMDS signal analysis, and NAMD theoretical methods (PDF)

AUTHOR INFORMATION

Corresponding Authors

Albert Liu − *Condensed Matter and Materials Science Division, Brookhaven National Laboratory, Upton, New York 11973, United States*; Email: aliu1@bnl.gov

Patanjali Kambhampati − *Department of Chemistry, McGill University, Montreal H3A 0B8, Canada*; orcid.org/0000-0003-0146-3544; Phone: +1-514-398-7228; Email: pat.kambhampati@mcgill.ca

Authors

Arnab Ghosh − *Department of Chemistry, McGill University, Montreal H3A 0B8, Canada*; orcid.org/0000-0001-9314-3059

Simon C. Boehme − *Department of Chemistry and Applied Biosciences, ETH Zürich, Zürich CH-8093, Switzerland; Laboratory for Thin Films and Photovoltaics, Empa - Swiss Federal Laboratories for Materials Science and Technology, Dübendorf CH-8600, Switzerland*; orcid.org/0000-0002-8399-5773

Patrick Brosseau − *Department of Chemistry, McGill University, Montreal H3A 0B8, Canada*

Dmitry N. Dirin − *Department of Chemistry and Applied Biosciences, ETH Zürich, Zürich CH-8093, Switzerland; Laboratory for Thin Films and Photovoltaics, Empa - Swiss Federal Laboratories for Materials Science and Technology, Dübendorf CH-8600, Switzerland*; orcid.org/0000-0002-5187-4555

Maksym V. Kovalenko − *Department of Chemistry and Applied Biosciences, ETH Zürich, Zürich CH-8093, Switzerland; Laboratory for Thin Films and Photovoltaics, Empa - Swiss Federal Laboratories for Materials Science and Technology, Dübendorf CH-8600, Switzerland*; orcid.org/0000-0002-6396-8938

Complete contact information is available at: https://pubs.acs.org/10.1021/acsnano.5c03051

Author Contributions

P.K. supervised the spectroscopy research. M.V.K. supervised the synthesis research. A.G. and P.B. conducted the CMDS experiments. A.G. performed the analysis of the CMDS experiments. A.L. performed the simulations. D.D. synthesized and characterized the LHP QDs. S.C.B. assisted in analysis and discussion. A.L. and P.K. wrote the manuscript with contributions from all authors.

Notes

The authors declare no competing financial interest.

ACKNOWLEDGMENTS

P.K. acknowledges financial support from CFI, NSERC, and Sony. A.L. was supported by the U.S. Department of Energy, Office of Basic Energy Sciences, under Contract No. DE-SC0012704. M.K. acknowledges financial support from the European Research Council through the European Union's Horizon 2020 programme (ERC Consolidator Grant SCALE-HALO, agreement no. 819740). The authors gratefully acknowledge the access to the Scientific Center for Optical and Electron Microscopy (ScopeM) at ETH Zürich and the Electron Microscopy Center at Empa. The authors are thankful to Dr. Frank Krumeich and Dr. Ihor Cherniukh for their help with taking electron microscopy images. The authors gratefully acknowledge the ScopeM facility at ETH Zürich for their support and assistance in this work.

REFERENCES

(1) Zhu, J.; Li, Y.; Lin, X.; Han, Y.; Wu, K. Coherent phenomena and dynamics of lead halide perovskite nanocrystals for quantum information technologies. *Nat. Mater.* **2024**, *23* (8), 1027−1040.

(2) Utzat, H.; Sun, W.; Kaplan, A. E. K.; Krieg, F.; Ginterseder, M.; Spokoyny, B.; Klein, N. D.; Shulenberger, K. E.; Perkinson, C. F.; Kovalenko, M. V.; et al. Coherent Single-Photon Emission from Colloidal Lead Halide Perovskite Quantum Dots. *Science* **2019**, *363*, 1068.

(3) Park, Y. S.; Guo, S.; Makarov, N. S.; Klimov, V. I. Room Temperature Single-Photon Emission from Individual Perovskite Quantum Dots. *ACS Nano* **2015**, *9*, 10386.

(4) Kaplan, A. E. K.; Krajewska, C. J.; Proppe, A. H.; Sun, W.; Sverko, T.; Berkinsky, D. B.; Utzat, H.; Bawendi, M. G. Hong−Ou−Mandel interference in colloidal CsPbBr3 perovskite nanocrystals. *Nat. Photonics* **2023**, *17*, 775.

(5) Rainò, G.; Becker, M. A.; Bodnarchuk, M. I.; Mahrt, R. F.; Kovalenko, M. V.; Stöferle, T. Superfluorescence from lead halide perovskite quantum dot superlattices. *Nature* **2018**, *563* (7733), 671−675.

(6) Russ, B.; Eisler, C. N. The future of quantum technologies: superfluorescence from solution-processed, tunable materials. *Nanophotonics* **2024**, *13* (11), 1943−1951.

(7) Zhu, C.; Boehme, S. C.; Feld, L. G.; Moskalenko, A.; Dirin, D. N.; Mahrt, R. F.; Stöferle, T.; Bodnarchuk, M. I.; Efros, A. L.; Sercel, P. C.; Kovalenko, M. V.; Rainò, G. Single-photon superradiance in individual caesium lead halide quantum dots. *Nature* **2024**, *626* (7999), 535−541.

(8) Liu, A.; Bonato, L. G.; Sessa, F.; Almeida, D. B.; Isele, E.; Nagamine, G.; Zagonel, L. F.; Nogueira, A. F.; Padilha, L. A.; Cundiff, S. T. Effect of dimensionality on the optical absorption properties of CsPbI3 perovskite nanocrystals. *J. Chem. Phys.* **2019**, *151* (19), No. 191103.

(9) Akkerman, Q. A.; Rainò, G.; Kovalenko, M. V.; Manna, L. Genesis, Challenges and Opportunities for Colloidal Lead Halide Perovskite Nanocrystals. *Nat. Mater.* **2018**, *17*, 394.

(10) Kovalenko, M. V.; Protesescu, L.; Bodnarchuk, M. I. Properties and Potential Optoelectronic Applications of Lead Halide Perovskite Nanocrystals. *Science* **2017**, *358*, 745.

(11) Bujalance, C.; Caliò, L.; Dirin, D. N.; Tiede, D. O.; Galisteo-López, J. F.; Feist, J.; García-Vidal, F. J.; Kovalenko, M. V.; Miguez, H. Strong light-matter coupling in lead halide perovskite quantum dot solids. *ACS Nano* **2023**, *18*, 4922.
(12) Dey, A.; Ye, J.; De, A.; Debroye, E.; Ha, S. K.; Bladt, E.; Kshirsagar, A. S.; Wang, Z.; Yin, J.; Wang, Y.; et al. State of the Art and Prospects for Halide Perovskite Nanocrystals. *ACS Nano* **2021**, *15* (7), 10775−10981.
(13) Rainò, G.; Yazdani, N.; Boehme, S. C.; Kober-Czerny, M.; Zhu, C.; Krieg, F.; Rossell, M. D.; Erni, R.; Wood, V.; Infante, I.; Kovalenko, M. V. Ultra-narrow room-temperature emission from single CsPbBr 3 perovskite quantum dots. *Nat. Commun.* **2022**, *13* (1), 2587.
(14) Protesescu, L.; Yakunin, S.; Bodnarchuk, M. I.; Krieg, F.; Caputo, R.; Hendon, C. H.; Yang, R. X.; Walsh, A.; Kovalenko, M. V. Nanocrystals of Cesium Lead Halide Perovskites (CsPbX3, X = Cl, Br, and I): Novel Optoelectronic Materials Showing Bright Emission with Wide Color Gamut. *Nano Lett.* **2015**, *15*, 3692.
(15) Akkerman, Q. A.; Nguyen, T. P. T.; Boehme, S. C.; Montanarella, F.; Dirin, D. N.; Wechsler, P.; Beiglböck, F.; Rainò, G.; Erni, R.; Katan, C.; Even, J.; Kovalenko, M. V. Controlling the nucleation and growth kinetics of lead halide perovskite quantum dots. *Science* **2022**, *377* (6613), 1406−1412.
(16) Ghosh, A.; Mora Perez, C.; Brosseau, P.; Dirin, D. N.; Prezhdo, O. V.; Kovalenko, M. V.; Kambhampati, P. Coherent Multidimensional Spectroscopy Reveals Hot Exciton Cooling Landscapes in CsPbBr3 Quantum Dots. *ACS Nano* **2025**, *19*, 14499.
(17) Kambhampati, P. Unraveling the excitonics of light emission from metal-halide perovskite quantum dots. *Nanoscale* **2024**, *16* (32), 15033−15058.
(18) Strandell, D. P.; Zenatti, D.; Nagpal, P.; Ghosh, A.; Dirin, D. N.; Kovalenko, M. V.; Kambhampati, P. Hot Excitons Cool in Metal Halide Perovskite Nanocrystals as Fast as CdSe Nanocrystals. *ACS Nano* **2023**, *18*, 1054.
(19) Strandell, D. P.; Kambhampati, P. Light Emission from CsPbBr 3 Metal Halide Perovskite Nanocrystals Arises from Dual Emitting States with Distinct Lattice Couplings. *Nano Lett.* **2023**, *23* (23), 11330−11336.
(20) Strandell, D. P.; Kambhampati, P. Observing strongly confined multiexcitons in bulk-like CsPbBr3 nanocrystals. *J. Chem. Phys.* **2023**, *158* (15), No. 154702.
(21) Strandell, D.; Perez, C. M.; Wu, Y.; Prezhdo, O. V.; Kambhampati, P. Excitonic Quantum Coherence in Light Emission from CsPbBr 3 Metal-Halide Perovskite Nanocrystals. *Nano Lett.* **2023**, *24*, 61.
(22) Strandell, D.; Wu, Y.; Mora-Perez, C.; Prezhdo, O.; Kambhampati, P. Breaking the Condon Approximation for Light Emission from Metal Halide Perovskite Nanocrystals. *J. Phys. Chem. Lett.* **2023**, *14*, 11281−11285.
(23) Strandell, D.; Dirin, D.; Zenatti, D.; Nagpal, P.; Ghosh, A.; Raino, G.; Kovalenko, M. V.; Kambhampati, P. Enhancing Multi-excitonic Emission in Metal-Halide Perovskites by Quantum Confinement. *ACS Nano* **2023**, *17*, 24910.
(24) Li, B.; Brosseau, P. J.; Strandell, D. P.; Mack, T. G.; Kambhampati, P. Photophysical Action Spectra of Emission from Semiconductor Nanocrystals Reveal Violations to the Vavilov Rule Behavior from Hot Carrier Effects. *J. Phys. Chem. C* **2019**, *123*, 5092.
(25) Fresch, E.; Camargo, F. V. A.; Shen, Q.; Bellora, C. C.; Pullerits, T.; Engel, G. S.; Cerullo, G.; Collini, E. Two-dimensional electronic spectroscopy. *Nat. Rev. Methods Primers* **2023**, 3 (1), 84.
(26) Biswas, S.; Kim, J.; Zhang, X.; Scholes, G. D. Coherent two-dimensional and broadband electronic spectroscopies. *Chem. Rev.* **2022**, *122* (3), 4257−4321.
(27) Seiler, H.; Palato, S.; Sonnichsen, C.; Baker, H.; Socie, E.; Strandell, D. P.; Kambhampati, P. Two-dimensional electronic spectroscopy reveals liquid-like lineshape dynamics in CsPbI3 perovskite nanocrystals. *Nat. Commun.* **2019**, *10*, 4962.
(28) Liu, A.; Almeida, D. B.; Bonato, L. G.; Nagamine, G.; Zagonel, L. F.; Nogueira, A. F.; Padilha, L. A.; Cundiff, S. T. Multidimensional coherent spectroscopy reveals triplet state coherences in cesium lead-halide perovskite nanocrystals. Science. *Advances* **2021**, *7* (1), No. eabb3594.
(29) Kambhampati, P. Hot Exciton Relaxation Dynamics in Semiconductor Quantum Dots: Radiationless Transitions on the Nanoscale. *J. Phys. Chem. C* **2011**, *115*, 22089.
(30) Kambhampati, P. Unraveling the structure and dynamics of excitons in semiconductor quantum dots. *Acc. Chem. Res.* **2011**, *44* (1), 1.
(31) Brosseau, P.; Jasrasaria, D.; Ghosh, A.; Seiler, H.; Palato, S.; Kambhampati, P. Two-Dimensional Electronic Spectroscopy Reveals Dynamics within the Bright Fine Structure of CdSe Quantum Dots. *J. Phys. Chem. Lett.* **2024**, *15* (6), 1702−1707.
(32) Brosseau, P. J.; Geuchies, J. J.; Jasrasaria, D.; Houtepen, A. J.; Rabani, E.; Kambhampati, P. Ultrafast hole relaxation dynamics in quantum dots revealed by two-dimensional electronic spectroscopy. *Commun. Phys.* **2023**, *6* (1), 48.
(33) Brosseau, P.; Ghosh, A.; Seiler, H.; Strandell, D.; Kambhampati, P. Exciton−polaron interactions in metal halide perovskite nanocrystals revealed via two-dimensional electronic spectroscopy. *J. Chem. Phys.* **2023**, *159* (18), No. 184711.
(34) Scholes, G. D. Coherence from light harvesting to chemistry. *J. Phys. Chem. Lett.* **2018**, *9*, 1568−1572.
(35) Maiuri, M.; Garavelli, M.; Cerullo, G. Ultrafast spectroscopy: State of the art and open challenges. *J. Am. Chem. Soc.* **2020**, *142* (1), 3−15.
(36) Scholes, G. D.; Fleming, G. R.; Chen, L. X.; Aspuru-Guzik, A.; Buchleitner, A.; Coker, D. F.; Engel, G. S.; van Grondelle, R.; Ishizaki, A.; Jonas, D. M.; Lundeen, J. S.; McCusker, J. K.; Mukamel, S.; Ogilvie, J. P.; Olaya-Castro, A.; Ratner, M. A.; Spano, F. C.; Whaley, K. B.; Zhu, X. Using coherence to enhance function in chemical and biophysical systems. *Nature* **2017**, *543* (7647), 647−656.
(37) Ball, P. Still seeking coherence. *Nat. Mater.* **2018**, *17* (3), 220−220.
(38) Cao, J.; Cogdell, R. J.; Coker, D. F.; Duan, H. G.; Hauer, J.; Kleinekathöfer, U.; Jansen, T. L. C.; Mančal, T.; Miller, R. J. D.; Ogilvie, J. P.; Prokhorenko, V. I.; Renger, T.; Tan, H. S.; Tempelaar, R.; Thorwart, M.; Thyrhaug, E.; Westenhoff, S.; Zigmantas, D. Quantum biology revisited. *Sci. Adv.* **2020**, *6* (14), No. eaaz4888.
(39) Engel, G. S.; Calhoun, T. R.; Read, E. L.; Ahn, T.-K.; Mančal, T.; Cheng, Y.-C.; Blankenship, R. E.; Fleming, G. R. Evidence for wavelike energy transfer through quantum coherence in photosynthetic systems. *Nature* **2007**, *446* (7137), 782−786.
(40) Collini, E.; Wong, C. Y.; Wilk, K. E.; Curmi, P. M.; Brumer, P.; Scholes, G. D. Coherently wired light-harvesting in photosynthetic marine algae at ambient temperature. *Nature* **2010**, *463* (7281), 644−647.
(41) Panitchayangkoon, G.; Hayes, D.; Fransted, K. A.; Caram, J. R.; Harel, E.; Wen, J.; Blankenship, R. E.; Engel, G. S. Long-lived quantum coherence in photosynthetic complexes at physiological temperature. *Proc. Natl. Acad. Sci. U. S. A.* **2010**, *107* (29), 12766−12770.
(42) Panitchayangkoon, G.; Voronine, D. V.; Abramavicius, D.; Caram, J. R.; Lewis, N. H.; Mukamel, S.; Engel, G. S. Direct evidence of quantum transport in photosynthetic light-harvesting complexes. *Proc. Natl. Acad. Sci. U. S. A.* **2011**, *108* (52), 20908−20912.
(43) Zhu, R.; Li, W.; Zhen, Z.; Zou, J.; Liao, G.; Wang, J.; Wang, Z.; Chen, H.; Qin, S.; Weng, Y. Quantum phase synchronization via exciton-vibrational energy dissipation sustains long-lived coherence in photosynthetic antennas. *Nat. Commun.* **2024**, *15* (1), 3171.
(44) Collini, E.; Scholes, G. D. Coherent intrachain energy migration in a conjugated polymer at room temperature. *science* **2009**, *323* (5912), 369−373.
(45) Halpin, A.; Johnson, P. J.; Tempelaar, R.; Murphy, R. S.; Knoester, J.; Jansen, T. L.; Miller, R. D. Two-dimensional spectroscopy of a molecular dimer unveils the effects of vibronic coupling on exciton coherences. *Nature Chem.* **2014**, *6* (3), 196−201.
(46) Duan, H.-G.; Prokhorenko, V. I.; Cogdell, R. J.; Ashraf, K.; Stevens, A. L.; Thorwart, M.; Miller, R. D. Nature does not rely on

https://doi.org/10.1021/acsnano.5c03051
ACS Nano 2025, 19, 19927−19937

long-lived electronic quantum coherence for photosynthetic energy transfer. *Proc. Natl. Acad. Sci. U. S. A.* **2017**, *114* (32), 8493−8498.
(47) Cassette, E.; Pensack, R. D.; Mahler, B.; Scholes, G. D. Room-temperature exciton coherence and dephasing in two-dimensional nanostructures. *Nat. Commun.* **2015**, *6* (1), 6086.
(48) Sonnichsen, C. D.; Strandell, D. P.; Brosseau, P. J.; Kambhampati, P. Polaronic quantum confinement in bulk CsPbBr 3 perovskite crystals revealed by state-resolved pump/probe spectroscopy. *Physical Review Research* **2021**, 3 (2), No. 023147.
(49) Kambhampati, P. Learning about the Structural Dynamics of Semiconductor Perovskites from Electron Solvation Dynamics. *J. Phys. Chem. C* **2021**, *125* (43), 23571−23586.
(50) Zhu, H. M.; Miyata, K.; Fu, Y. P.; Wang, J.; Joshi, P. P.; Niesner, D.; Williams, K. W.; Jin, S.; Zhu, X. Y. Screening in crystalline liquids protects energetic carriers in hybrid perovskites. *Science* **2016**, *353* (6306), 1409.
(51) Miyata, K.; Meggiolaro, D.; Trinh, M. T.; Joshi, P. P.; Mosconi, E.; Jones, S. C.; De Angelis, F.; Zhu, X. Y. Large Polarons in Lead Halide Perovskites. *Sci. Adv.* **2017**, *3*, No. e1701217.
(52) Miyata, K.; Atallah, T. L.; Zhu, X. Y. Lead Halide Perovskites: Crystal-Liquid Duality, Phonon Glass Electron Crystals, and Large Polaron Formation. *Sci. Adv.* **2017**, *3*, No. e1701469.
(53) Wu, X.; Tan, L. Z.; Shen, X.; Hu, T.; Miyata, K.; Trinh, M. T.; Li, R.; Coffee, R.; Liu, S.; Egger, D. A.; Makasyuk, I.; Zheng, Q.; Fry, A.; Robinson, J. S.; Smith, M. D.; Guzelturk, B.; Karunadasa, H. I.; Wang, X.; Zhu, X.; Kronik, L.; Rappe, A. M.; Lindenberg, A. M. Light-induced picosecond rotational disordering of the inorganic sublattice in hybrid perovskites. *Sci. Adv.* **2017**, *3* (7), No. e1602388.
(54) Guo, Y.; Yaffe, O.; Hull, T. D.; Owen, J. S.; Reichman, D. R.; Brus, L. E. Dynamic emission Stokes shift and liquid-like dielectric solvation of band edge carriers in lead-halide perovskites. *Nat. Commun.* **2019**, *10*, 1175.
(55) Yaffe, O.; Guo, Y. S.; Tan, L. Z.; Egger, D. A.; Hull, T.; Stoumpos, C. C.; Zheng, F.; Heinz, T. F.; Kronik, L.; Kanatzidis, M. G.; et al. Local Polar Fluctuations in Lead Halide Perovskite Crystals. *Phys. Rev. Lett.* **2017**, *118* (13), No. 136001.
(56) Ghosh, S.; Rana, D.; Pradhan, B.; Donfack, P.; Hofkens, J.; Materny, A. Vibrational study of lead bromide perovskite materials with variable cations based on Raman spectroscopy and density functional theory. *J. Raman Spectrosc.* **2021**, *52* (12), 2338−2347.
(57) Feld, L. G.; Boehme, S. C.; Sabisch, S.; Frenkel, N.; Yazdani, N.; Morad, V.; Zhu, C.; Svyrydenko, M.; Tao, R.; Bodnarchuk, M. Phonon-driven wavefunction localization promotes room-temperature, pure single-photon emission in large organic-inorganic lead-halide quantum dots. *arXiv* **2024**, https://arxiv.org/abs/2404.15920.
(58) Ghosh, A.; Strandell, D. P.; Kambhampati, P. A spectroscopic overview of the differences between the absorbing states and the emitting states in semiconductor perovskite nanocrystals. *Nanoscale* **2023**, *15* (6), 2470.
(59) Zhu, C.; Feld, L. G.; Svyrydenko, M.; Cherniukh, I.; Dirin, D. N.; Bodnarchuk, M. I.; Wood, V.; Yazdani, N.; Boehme, S. C.; Kovalenko, M. V.; Rainò, G.; et al. Quantifying the Size-Dependent Exciton-Phonon Coupling Strength in Single Lead-Halide Perovskite Quantum Dots. *Adv. Opt. Mater.* **2024**, *12* (8), No. 2301534.
(60) Palato, S.; Seiler, H.; Nijjar, P.; Prezhdo, O.; Kambhampati, P. Atomic fluctuations in electronic materials revealed by dephasing. *Proc. Natl. Acad. Sci. U. S. A.* **2020**, *117* (22), 11940.
(61) Brosseau, P.; Seiler, H.; Palato, S.; Sonnichsen, C.; Baker, H.; Socie, E.; Strandell, D.; Kambhampati, P. Perturbed free induction decay obscures early time dynamics in two-dimensional electronic spectroscopy: The case of semiconductor nanocrystals. *J. Chem. Phys.* **2023**, *158* (8), No. 084201.
(62) Palato, S.; Seiler, H.; Baker, H.; Sonnichsen, C.; Brosseau, P.; Kambhampati, P. Investigating the electronic structure of confined multiexcitons with nonlinear spectroscopies. *J. Chem. Phys.* **2020**, *152* (10), 21.
(63) Brosseau, P.; Palato, S.; Seiler, H.; Baker, H.; Kambhampati, P. Fifth-order two-quantum absorptive two-dimensional electronic spectroscopy of CdSe quantum dots. *J. Chem. Phys.* **2020**, *153* (23), No. 234703.
(64) Seiler, H.; Palato, S.; Sonnichsen, C.; Baker, H.; Kambhampati, P. Seeing Multiexcitons through Sample Inhomogeneity: Band-Edge Biexciton Structure in CdSe Nanocrystals Revealed by Two-Dimensional Electronic Spectroscopy. *Nano Lett.* **2018**, *18*, 2999.
(65) Seiler, H.; Palato, S.; Kambhampati, P. Investigating exciton structure and dynamics in colloidal CdSe quantum dots with two-dimensional electronic spectroscopy. *J. Chem. Phys.* **2018**, *149* (7), No. 074702.
(66) Efros, A. L.; Brus, L. E. Nanocrystal Quantum Dots: From Discovery to Modern Development. *ACS Nano* **2021**, *15*, 6192.
(67) Efros, A. L.; Rosen, M. The electronic structure of semiconductor nanocrystals. *Annu. Rev. Mater. Sci.* **2000**, *30* (1), 475−521.
(68) Jasrasaria, D.; Rabani, E. Circumventing the phonon bottleneck by multiphonon-mediated hot exciton cooling at the nanoscale. *npj Computational Materials* **2023**, *9* (1), 145.
(69) Jasrasaria, D.; Weinberg, D.; Philbin, J. P.; Rabani, E. Simulations of nonradiative processes in semiconductor nanocrystals. *J. Chem. Phys.* **2022**, *157* (2), No. 020901.
(70) Jasrasaria, D.; Rabani, E. Interplay of surface and interior modes in exciton−phonon coupling at the nanoscale. *Nano Lett.* **2021**, *21* (20), 8741−8748.
(71) Guzelturk, B.; Cotts, B. L.; Jasrasaria, D.; Philbin, J. P.; Hanifi, D. A.; Koscher, B. A.; Balan, A. D.; Curling, E.; Zajac, M.; Park, S.; et al. Dynamic lattice distortions driven by surface trapping in semiconductor nanocrystals. *Nat. Commun.* **2021**, *12* (1), 1860.
(72) Prezhdo, O. V. Modeling non-adiabatic dynamics in nanoscale and condensed matter systems. *Acc. Chem. Res.* **2021**, *54* (23), 4239−4249.
(73) Neukirch, A. J.; Hyeon-Deuk, K.; Prezhdo, O. V. Time-Domain Ab Initio Modeling of Excitation Dynamics in Quantum Dots. *Coord. Chem. Rev.* **2014**, *263*−*264*, 161.
(74) Kilina, S. V.; Kilin, D. S.; Prezhdo, O. V. Breaking the Phonon Bottleneck in PbSe and CdSe Quantum Dots: Time-Domain Density Functional Theory of Charge Carrier Relaxation. *ACS Nano* **2009**, *3*, 93.
(75) Sagar, D. M.; Cooney, R. R.; Sewall, S. L.; Dias, E. A.; Barsan, M. M.; Butler, I. S.; Kambhampati, P. Size dependent, state-resolved studies of exciton-phonon couplings in strongly confined semiconductor quantum dots. *Phys. Rev. B: Condens. Matter Mater. Phys.* **2008**, *77* (23), No. 235321.
(76) Walsh, B. R.; Sonnichsen, C.; Mack, T. G.; Saari, J. I.; Krause, M. M.; Nick, R.; Coe-Sullivan, S.; Kambhampati, P. Excited State Phononic Processes in Semiconductor Nanocrystals Revealed by Excitonic State-Resolved Pump/Probe Spectroscopy. *J. Phys. Chem. C* **2019**, *123* (6), 3868−3875.
(77) Sewall, S. L.; Franceschetti, A.; Cooney, R. R.; Zunger, A.; Kambhampati, P. Direct observation of the structure of band-edge biexcitons in colloidal semiconductor CdSe quantum dots. *Phys. Rev. B* **2009**, *80* (8), 4.
(78) Sewall, S. L.; Cooney, R. R.; Kambhampati, P. Experimental tests of effective mass and atomistic approaches to quantum dot electronic structure: Ordering of electronic states. *Appl. Phys. Lett.* **2009**, *94* (24), 3.
(79) Seibt, J.; Hansen, T.; Pullerits, T. 3D Spectroscopy of Vibrational Coherences in Quantum Dots: Theory. *J. Phys. Chem. B* **2013**, *117* (38), 11124−11133.
(80) Seibt, J.; Pullerits, T. Beating Signals in 2D Spectroscopy: Electronic or Nuclear Coherences? Application to a Quantum Dot Model System. *J. Phys. Chem. C* **2013**, *117* (36), 18728−18737.
(81) Butkus, V.; Valkunas, L.; Abramavicius, D. Molecular vibrations-induced quantum beats in two-dimensional electronic spectroscopy. *J. Chem. Phys.* **2012**, *137* (4), No. 044513.
(82) Tsubouchi, M.; Ishii, N.; Kagotani, Y.; Shimizu, R.; Fujita, T.; Adachi, M.; Itakura, R. Beat-frequency-resolved two-dimensional electronic spectroscopy: disentangling vibrational coherences in

artificial fluorescent proteins with sub-10-fs visible laser pulses. *Opt. Express* **2023**, *31* (4), 6890−6906.
(83) Cundiff, S. T.; Mukamel, S. Optical multidimensional coherent spectroscopy. *Phys. Today* **2013**, *66* (7), 44−49.
(84) Strandell, D. P.; Ghosh, A.; Zenatti, D.; Nagpal, P.; Kambhampati, P. Direct Observation of Higher Multiexciton Formation and Annihilation in CdSe Quantum Dots. *J. Phys. Chem. Lett.* **2023**, *14* (30), 6904−6911.
(85) Saari, J. I.; Dias, E. A.; Reifsnyder, D.; Krause, M. M.; Walsh, B. R.; Murray, C. B.; Kambhampati, P. Ultrafast Electron Trapping at the Surface of Semiconductor Nanocrystals: Excitonic and Biexcitonic Processes. *J. Phys. Chem. B* **2013**, *117* (16), 4412−4421.
(86) Kambhampati, P. Multiexcitons in Semiconductor Nanocrystals: A Platform for Optoelectronics at High Carrier Concentration. *J. Phys. Chem. Lett.* **2012**, *3* (9), 1182.
(87) Tyagi, P.; Kambhampati, P. False multiple exciton recombination and multiple exciton generation signals in semiconductor quantum dots arise from surface charge trapping. *J. Chem. Phys.* **2011**, *134* (9), 10.
(88) Sewall, S. L.; Cooney, R. R.; Dias, E. A.; Tyagi, P.; Kambhampati, P. State-resolved observation in real time of the structural dynamics of multiexcitons in semiconductor nanocrystals. *Phys. Rev. B* **2011**, *84* (23), 8.
(89) Sewall, S. L.; Cooney, R. R.; Anderson, K. E. H.; Dias, E. A.; Sagar, D. M.; Kambhampati, P. State-resolved studies of biexcitons and surface trapping dynamics in semiconductor quantum dots. *J. Chem. Phys.* **2008**, *129* (8), No. 084701.
(90) Sewall, S. L.; Cooney, R. R.; Anderson, K. E. H.; Dias, E. A.; Kambhampati, P. State-to-state exciton dynamics in semiconductor quantum dots. *Phys. Rev. B: Condens. Matter Mater. Phys.* **2006**, *74* (23), No. 235328.
(91) Mukamel, S. *Principles of nonlinear optical spectroscopy*; Oxford University Press: USA, 1995.
(92) Li, H.; Lomsadze, B.; Moody, G.; Smallwood, C.; Cundiff, S. *Optical Multidimensional Coherent Spectroscopy*; Oxford University Press: 2023.
(93) Zanni, M.; Hamm, P. *Concepts and Methods of 2D Infrared Spectroscopy*; Cambridge University Press: 2011.
(94) Sonnichsen, C.; Brosseau, P.; Reid, C.; Kambhampati, P. OPA-driven hollow-core fiber as a tunable, broadband source for coherent multidimensional spectroscopy. *Opt. Express* **2021**, *29* (18), 28352−28358.
(95) Palato, S.; Seiler, H.; Baker, H.; Sonnichsen, C.; Zifkin, R.; McGowan, J.; Kambhampati, P. An analysis of hollow-core fiber for applications in coherent femtosecond spectroscopies. *J. Appl. Phys.* **2020**, *128* (10), No. 103107.
(96) Seiler, H.; Palato, S.; Schmidt, B. E.; Kambhampati, P. Simple fiber-based solution for coherent multidimensional spectroscopy in the visible regime. *Opt. Lett.* **2017**, *42* (3), 643.
(97) Seiler, H.; Palato, S.; Kambhampati, P. Coherent multidimensional spectroscopy at optical frequencies in a single beam with optical readout. *J. Chem. Phys.* **2017**, *147* (9), No. 094203.
(98) Seiler, H.; Walsh, B.; Palato, S.; Thai, A.; Crozatier, V.; Forget, N.; Kambhampati, P. Kilohertz generation of high contrast polarization states for visible femtosecond pulses via phase-locked acousto-optic pulse shapers. *J. Appl. Phys.* **2015**, *118* (10), No. 103110.

https://doi.org/10.1021/acsnano.5c03051
ACS Nano 2025, 19, 19927−19937